Design and Development of a Lightweight, High-Torque, and Cost-Effective Hip exoskeleton

Jose Esquivel Patricio, Mojtaba Sharifi, *Member, IEEE*, Dhurba Shrestha, Sai Hein Si Thu, and Eric Kwan

Abstract—Individuals with physical impairments and chronic conditions (including children, adolescents, adults, and seniors) who have motor disabilities are recommended to use assistive devices to perform activities of daily living (ADLs). Developing these devices to be cost-effective, lightweight, and comfortable would make them more practical for home-based usage with a significant impact on people's lives. In this work, a new hip exoskeleton is designed with low weight and cost while ensuring the wearer's comfort in various movements. In addition, this exoskeleton maintains high structural strength and torque power. This lower limb exoskeleton has two degrees of freedom (DOFs) and can generate hip movement trajectories in the sagittal plane. The structure of this exoskeleton was fabricated from light and printable materials such as thermoplastic polyurethane (TPU), Polyethylene terephthalate glycol (PETG), polylactic acid (PLA), and carbon fiber to make it more affordable for a larger population of end-users. A compact control system including a high-torque DC motor, mini-PC, microcontroller, and intermediate boards was carefully selected to optimize the size of this device. Experimental studies have been performed to evaluate the performance of this exoskeleton in walking and sit-to-stand movements at low and high speeds.

Index Terms—Hip exoskeleton, Human-robot interaction, Assistive device, Hardware and software development, Lower-limb movements

I. INTRODUCTION

Spinal Cord Injuries (SCI) and stroke can lead to neurological conditions and physical impairments [1]. An analysis from the National SCI Database (NSCID) reported that from 2005 to 2011, SCIs were caused by shootings (10.4%), automobile accidents (31.5%), falling (25.3%), and motorcycle accidents (6.8%) [2]. Elderly people with chronic conditions and motor disabilities experience difficulties in performing ADLs and moving around due to the deterioration of their locomotive capabilities [3]. Wearable robotic systems and exoskeletons have been developed to assist and rehabilitate these individuals and reduce their secondary complications.

Powered exoskeletons can deliver frequent, consistent, and long-term physical assistance with minimal engagement of a therapist or caregiver [4]. Employing these robotic systems may free a considerable amount of social labor, reduce the costs of healthcare, and ensure timelier ADLs support such as walking. Additionally, by embedding sensors in the structure of the exoskeleton, precise measurements can be collected of human limb movements for continuous monitoring of the user's condition. EksoNR, ReWalk Personal 6.0, Hybrid Assistive Limb (HAL), and Indego exoskeletons are some of the commercially available lower-limb exoskeletons [5]–[7]. Although these exoskeletons are now being used in some clinical settings [8], their heaviness, costs, and safety considerations have made them less practical for home-based and long-term assistance and rehabilitation [9]–[11]

Fully functioning exoskeletons also face mobility challenges because of desynchronization between the user and the machine [4]. In order to increase the reliability and precision of operating an exoskeleton, various control methods have been developed. Furthermore, because of differences in the functional capacity and behavior of users, variations in their intention during the task, and effects of environmental factors (slope and condition of the surface), establishing adaptable, safe, and comfortable HRI control requires an online investigation of physical human force/torque [12]–[14]. Consequently, it is crucial to determine the interaction force/torque between the human and exoskeleton in order to design high-level motion planning and low-level torque control systems. A common method of estimating HRI torque is to use EMG signals acquired from human muscles [15]–[19]. However, the obtained results are subject to considerable inaccuracy due to several factors, including calibration, muscle fatigue, electrode positioning, and variations in muscle-skin conductivity [20].

In order to overcome these issues, force/torque sensors have been utilized as an alternative solution in some research studies [4], [21]–[24]. Despite the accurate data of these sensors, their cost and difficulty in embedding them between the human body and exoskeleton drove researchers and manufacturers to rely more on estimation methods instead of direct measurement of the interaction force/torque. Dynamic modeling of musculoskeletal systems was also utilized to estimate the passive portion of the interaction torque [20], [21], [25], [26]; however, its active part is either neglected or estimated from force/torque measurements. To address these measurement challenges autonomously, disturbance observers were developed for online estimation of HRI torque [27]–[29]. Pan *et al.* [27] designed a nonlinear model-based observer to compensate for the external torque in their low-level controller for trajectory tracking. In other studies [29], [30], nonlinear disturbance observers were investigated to estimate the human torque, which was used in the proportional–derivative (PD) torque control law of lower-limb exoskeleton. In recent studies [30], [31], by incorporating HRI torque estimation in adaptive central pattern generators (CPGs), the amplitude, frequency, and phase of walking can be updated in accordance with the wearer's intention (physical behavior).

In this study, a lightweight and cost-effective hip exoskeleton is designed and fabricated for assistance, rehabilitation, and gait training applications. By incorporating lighter sturdy components and a compact mechatronic system, the weight of

this exoskeleton has been significantly reduced. The employed brushless DC motor (AK80-64) has a high output torque with a nominal magnitude of 48 Nm and a maximum magnitude of 120 Nm and an optimally compact design that makes it appropriate for this wearable device. 3D-printed components in lighter and softer materials such as polylactic acid (PLA), thermoplastic polyurethane (TPU), polyethylene terephthalate glycol (PETG), and carbon fiber have been employed to reduce the total weight of this exoskeleton. This design could improve the user's mobility and comfort at a low cost, which makes this assistive device highly affordable. A microcontroller and CAN boards are used to enable bilateral signal communication with the DC motors for sending commands and receiving feedback. In this work, a PD position controller is implemented to track repetitive locomotion trajectories and sit-to-stand movements at different speed levels (slow and fast). Based on the performance of this exoskeleton in different scenarios, the wearer can make modifications to motion characteristics such as speed and step size.

II. Design and Development of Hip Exoskeleton

This section covers the detailed design process used to develop the proposed hip exoskeleton. The components of this exoskeleton are illustrated in Fig. 1. The motors are secured by a cover and attached to the hip brace which is fastened around the user's trunk support component. As seen in Fig. 1, the front side of the motor is connected to the top section of the hip component (for torque transmission) using screws. Similarly, the bottom part of this long hip component is connected to the thigh brace so that the torque is transmitted to the thigh to generate the hip joint movements. The thigh brace is secured on the user's thigh using a flexible Velcro strap. Finally, the hip brace will be lined with soft fabric on the inner side for the wearer's comfort. Based on the concept, design, motor specs, and torque requirement of the hip exoskeleton, the initial CAD model of the hip components is created using SOLIDWORKS.

A. Structural design of the hip exoskeleton

The hip exoskeleton is designed to achieve three specific goals, i.e. lightweight, high torque, and cost-effectiveness. Two different initial designs of the hip exoskeleton are considered prior to this model (Fig. 1), first to analyze and reduce the stresses and strains on the components and second to elevate the users' experience. The CAD model of the hip component is designed based on a height of 5 ft 8 inches and a weight of 164 lbs for the wearer. The CAD models were analyzed in the SOLIDWORKS. To avoid alignment issues, the master model technique is used to create the model, and each component is exported for assembly. Various features in the SOLIDWORKS such as an extruded boss/cut, sweep, loft, surface features, and split are used to model the hip components of the exoskeleton. Materials are assigned to each component to evaluate the weight of the exoskeleton.

After finalizing the materials for the components of the hip exoskeleton, motors for the actuator, and torque required to support the hip exoskeleton, the CAD design of the initial
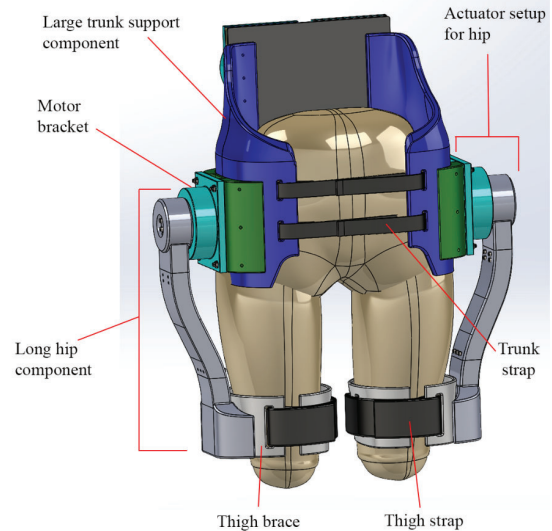

Fig. 1. CAD model of the developed hip exoskeleton: Front Isometric View

hip exoskeleton was revised. Figures 1 and 2 show the front isometric view and the back isometric view of this revised CAD model for this exoskeleton, respectively. In this design, additional components such as motors, motor covers, hip connectors, thigh brace, mounting screws, Velcro straps, hip brace, and back plate are included. Polylactic acid (PLA), thermoplastic polyurethane (TPU), and polyethylene terephthalate glycol (PETG) filaments are utilized for 3D printing different components. These components are designed such that they can support the maximum nominal torque from the motor (48 Nm) [32]. The large trunk support component (illustrated in Fig. 1) has a top curve that is designed to sit on the wearer's pelvis, which provides additional support from the wearer's trunk and avoid the whole assembly from sliding down. The back plate is designed from carbon fiber to have high strength for fixing four motors as additional actuators for the knee and ankle joints using a cable-driven system in the next generation of this device.

B. 3D-printed components of the hip exoskeleton

This section covers the 3D-Printed components of the hip exoskeleton in PLA material. Figure 3 shows the CAD model, 3D printed hip components, and thigh brace of the exoskeleton. The top circular part of the hip component that connects to the motor has dimensions of 3.5-inch diameter and 1.75-inch depth. Similarly, the rigid frame in the middle is made from a 2.75-inch width x 1.25-inch-thick rectangular bar and connects to the 4-inch by a 0.375-inch-thick thigh brace. Figure 3 demonstrates the exploded view of the three-part hip component that has been fixed together by screws. The thigh brace shown in Fig. 1 has a diameter of 7.25 inches and a height of 4 inches and it has been split into two parts and connected using Velcro thigh straps to be adjustable to different wearers.

The motor cover, hip connector, and large trunk support part are designed to secure the DC motor (AK80-64) to the trunk support component, illustrated in Fig. 1. All the parts
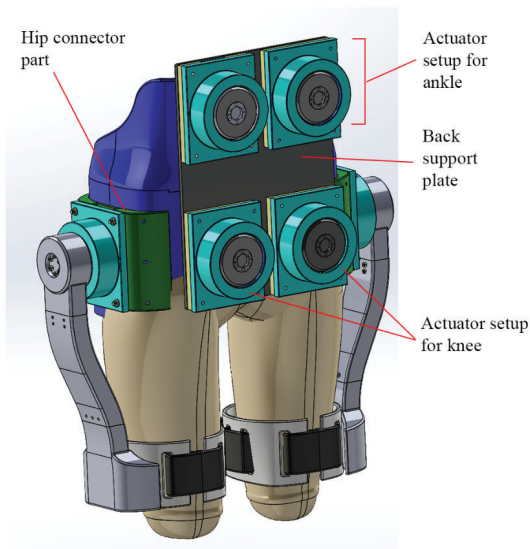
Fig. 2.   CAD model of the developed hip exoskeleton: Back Isometric View

Fig. 3.   Left: the exploded view of the hip component model. Center and Right: design assembly and 3D print of the hip component and thigh brace

are printed in PLA with 90-100 percent infill to support the maximum loading conditions properly. Figure 4 (a) shows the CAD model and 3D-printed hip connector part. The motor is connected from the back using machine screws to the trunk support component.

The large trunk support component has a curved surface at the upper section which is designed to sit on the user's pelvis to provide additional support and prevent it from sliding down from the hip. It has a dimension of 8.875-inch width x 3.75-inch depth x 15-inch height, which is the largest component
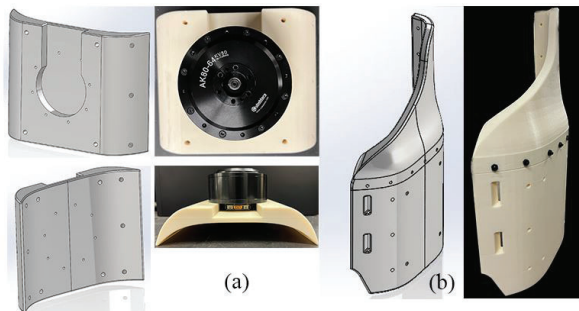

Fig. 4.   (a) CAD model and 3D printed hip connector part with AK80-64 Brushless DC motor mounted on, and (b) CAD model and 3D printed large trunk support component

in the hip exoskeleton 3D printed in PLA material. This part is a fixation base around the trunk that holds all the components together. Figure 4 (b) demonstrates the CAD model and 3D print of the large trunk support component for the right leg. Based on the conducted Finite Element Analysis (FEA), the maximum stress values for the long hip component, hip connector part, and large trunk support component are 4.84 MPa, 1.89 MPa, and 2.96 MPa, respectively, when a maximum torque of 48 N.m is applied by the motor. This makes the factor of safety more than 3.23 and the maximum deflection 0.147 mm occurring in the trunk support component.

III. MECHATRONICS DEVELOPMENT

In this section, a thorough breakdown of the mechatronic setup to test the developed hip exoskeleton is described. The control hardware of this exoskeleton includes a microcontroller, actuators, and intermediate boards, and a power supply, as shown in Fig. 5. The microcontroller for this exoskeleton's mechatronic system is the ESP-Wroom-32 with two cores and 240 MHz of memory speed. The SN65HVD230 CAN board (from AITRIP) is used as an intermediate board to communicate between the ESP 32 and the motor for sending and receiving CAN signals. This configuration (Fig. 5) enables a bilateral signal communication with the AK80-64 motors (from T-Motor) that has an input port for the CAN protocol. The RD6018 DC power supply, with an output voltage range of 44-60 volts, is used for testing purposes. An Intel NUC11PAHi7 mini-PC is utilized to execute the main c++ code for the control of the exoskeleton with the ESP32 microcontroller.

This lower-limb assistive exoskeleton has been designed to move the hip joints with the capability of applying the maximum torque needed to move the hip joint, which is reported 60 Nm [33]. The employed brushless DC motor (AK80-64) has a high output torque, a lightweight, and a compact design (Figs. 4, 5 and 6). This motor has a nominal torque of 48 Nm and a maximum peak torque of 120 Nm.

A. Hardware and software architecture

The experimental setup of the mechatronic system to control and test the motors is illustrated in Fig. 5. The employed power supply can deliver 48 V with a maximum current of 18 Amps to the motors. The ESP 32 microcontroller is connected to the CAN board to provide communication with the motor containing two 120 Ohm terminating resistors. As described in Fig. 6, the motor control program is written in C++ using Visual Studio and the PlatformIO IDE as the user interface. The program was developed based on the AK80-64 Series actuator driver manual v1.0.9 that includes steps to transfer the C++ program into CAN communication for driving the motor [34]. The motor sends back bits of data that had to be reorganized to obtain motor position, speed, current, temperature, and errors. Based on the manufacturer's recommendation and a trial-and-error approach to achieving appropriate tracking performance for hip movements, the position control parameters of the DC motor have been set at $k_p = 300$ N.m/rad and $K_d = 2$

N.m.sec/rad. This was according to the hip motion's amplitude and speed in different activities including walking and sit-to-stand. Note that the total cost of developing this exoskeleton including DC motors, a mini-PC, and materials was less than $3k.

IV. EXPERIMENTAL EVALUATIONS

The developed hip exoskeleton was tested experimentally in walking and sit-to-stand motions. For this purpose, the empirical data of typical lower limb walking and sit-to-stand trajectories were employed from the user studies in [35] and [36], respectively. The obtained hip trajectories were formulated by the Fourier series with 5-6 terms to generate time-continues desired profiles for the position controller of the AK80-64 motors. The desired trajectories $q_{w_i}(t)$ for the joint i of the exoskeleton were defined as

$$q_{des}(t) = a_0 + \sum_{k=1}^{N}(a_k \cos k\theta_i(t) + b_k \sin k\theta_i(t)) \quad (1)$$

where a_k and b_k are the coefficients of Fourier series with N terms. The values of these coefficients were identified to achieve the best fitting, with a minimum error compared to the empirical trajectories. These values are mentioned in Table I).

The actual position of the hip joint was obtained from the encoder embedded in the motor. The tracking performance of the exoskeleton in walking (with a frequency of 2.63 rad/sec) is illustrated in Fig. 7. As seen, four full strides were made in the span of 10 seconds and the maximum peak error was 0.066 rad between the desired and actual trajectory. This indicates a high accuracy for this typical speed of walking. As a result, the applied motor torque had a maximum of 19.6 Nm, as plotted in 8.

The hip exoskeleton was also tested in a sit-to-stand transition. The actual and desired hip trajectories in this movement scenario are shown in Figs. 9 and 10. The tracking performance of the exoskeleton in two different periods of this transition between the "sit" and "stand" states is demonstrated. With a 6-second window for this transition, the maximum tracking error was 0.035 rad in Figs. 9, which resulted in the highest motor torque of 10.53 Nm in Fig. 11. Moreover, when the sit-to-stand time window was decreased to 3 seconds (fast transition scenario), the maximum tracking error increased to 0.067 rad in Fig. 10, and the motor torque increased to 20.22 Nm in Fig. 11. Comparing these results indicates that higher sit-to-stand speed and acceleration of the hip trajectory can impact the tracking error and required torque magnitude.

V. CONCLUSION

In this study, we designed and developed a hip exoskeleton to be used as a mechatronic system for assistance and rehabilitation. This exoskeleton has been modeled, analyzed, and fabricated to meet the requirements of being lightweight and cost-effective, while it is capable of delivering high torque to the hip joint. The design process involved creating initial designs, analyzing them in SOLIDWORKS, and revising the components by various techniques such as extruded boss/cut, sweep, loft, surface features, and split. The materials used for 3D printing were selected based on the motor specifications and torque requirements (including the maximum torque of 48 Nm). The exoskeleton's assembly is comprised of several components including the hip brace, thigh brace, hip connector, motor cover, back plate, and large trunk support component. The 3D printed components were made using polylactic acid (PLA), thermoplastic polyurethane (TPU), and polyethylene terephthalate glycol (PETG) filaments with 90-100 percent infill to withstand maximum loading conditions.

This exoskeleton provides a wide range of mobility and torque rendering for the hip joint to assist people in lower limb activities. This device is a foundation for the development of a three-joint exoskeleton in the future including hip, knee, and ankle components. The AK80-64 DC motor was utilized and experimentally tested by tracking typical human hip motion trajectories for walking and sit-to-stand activities. Experimental results showed that the exoskeleton had a low tracking error (maximum 0.066 rad) at a typical speed of locomotion, indicating appropriate tracking performance. The motor torque for typical walking was less than 20 Nm. This performance was also evaluated in the sit-to-stand transition within two periods of 3 sec and 6 sec, which resulted in tracking errors of 0.035 rad and 0.067 rad. In future studies, the exoskeleton's control strategy will be developed to be adaptive in order to identify the wearer's intention and shape motion trajectories based on HRI torque estimation. Moreover, a light portable battery will be utilized to power this exoskeleton which is rechargeable to power the actuators and other electronic components.

REFERENCES

[1] "Spinal cord injury." [Online]. Available: https://www.ninds.nih.gov/Disorders/All-Disorders/Spinal-Cord-Injury-Information-Page

[2] Y. Chen, Y. Tang, L. Vogel, and M. DeVivo, "Causes of Spinal Cord Injury," *Topics in Spinal Cord Injury Rehabilitation*, vol. 19, no. 1, pp. 1–8, 01 2013. [Online]. Available: https://doi.org/10.1310/sci1901-1

[3] A. Kapsalyamov, P. K. Jamwal, S. Hussain, and M. H. Ghayesh, "State of the art lower limb robotic exoskeletons for elderly assistance," *IEEE Access*, vol. 7, pp. 95 075–95 086, 2019.

[4] H. Lee, P. W. Ferguson, and J. Rosen, "Chapter 11 - lower limb exoskeleton systems—overview," in *Wearable Robotics*, J. Rosen and P. W. Ferguson, Eds. Academic Press, 2020, pp. 207–229. [Online]. Available: https://www.sciencedirect.com/science/article/pii/B9780128146590000114

[5] S. A. Murray, R. J. Farris, M. Golfarb, C. Hartigan, C. Kandilakis, and D. Truex, "Fes coupled with a powered exoskeleton for cooperative muscle contribution in persons with paraplegia," in *2018 40th Annual International Conference of the IEEE Engineering in Medicine and Biology Society (EMBC)*, 2018, pp. 2788–2792.

[6] P. Stegall, K. Winfree, D. Zanotto, and S. K. Agrawal, "Rehabilitation exoskeleton design: Exploring the effect of the anterior lunge degree of freedom," *IEEE Transactions on Robotics*, vol. 29, no. 4, pp. 838–846, 2013.

[7] G. Zeilig, H. Weingarden, M. Zwecker, I. Dudkiewicz, A. Bloch, and A. Esquenazi, "Safety and tolerance of the rewalk™ exoskeleton suit for ambulation by people with complete spinal cord injury: A pilot study," *The Journal of Spinal Cord Medicine*, vol. 35, no. 2, pp. 96–101, 2012, pMID: 22333043.

[8] A. Esquenazi, M. Talaty, and A. Jayaraman, "Powered exoskeletons for walking assistance in persons with central nervous system injuries: A narrative review," *PMR*, vol. 9, no. 1, pp. 46–62, 2017.
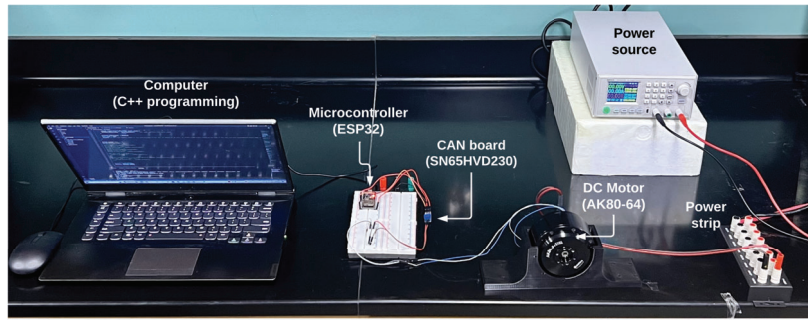
Fig. 5.   Experimental setup to test the control and actuation system including AK80-64 DC motors, ESP-Wroom-32 as the microcontroller and SN65HVD230 CAN board
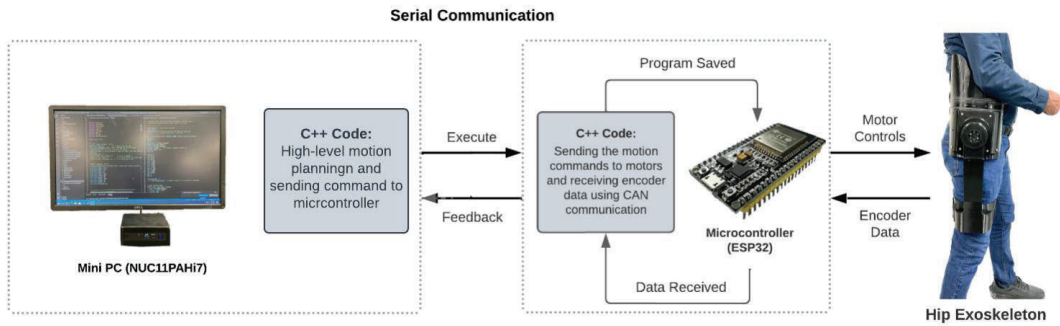

Fig. 6.   Architecture of the mechatronic hardware and software for the hip exoskeleton: C++ code is executed on PC for motion planning and C++ code is executed on the microcontroller for CAN communication with motors

TABLE I
COEFFICIENTS OF THE FOURIER SERIES FOR THE HIP WHILE WALKING AND FROM SITTING TO STANDING.*

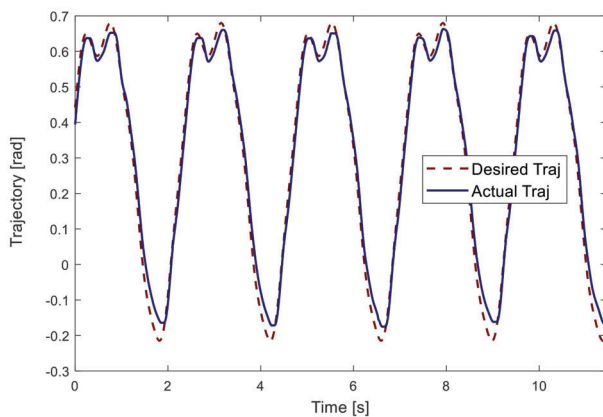| State	Joint	a_0	a_1	a_2	a_3	a_4	a_5	a_6	b_1	b_2	b_3	b_4	b_5	b_6
Walking	Hip	40.69	23.22	-4.49	0.40	0.70	1.08	-0.27	-8.65	3.34	1.39	0.80	0.34	0.07
Sit-to-Stand	Hip	49.59	22.01	-1.31	0.28	-0.72	0.15	n/a	35.11	-11.48	-4.05	-0.16	0.40	n/a

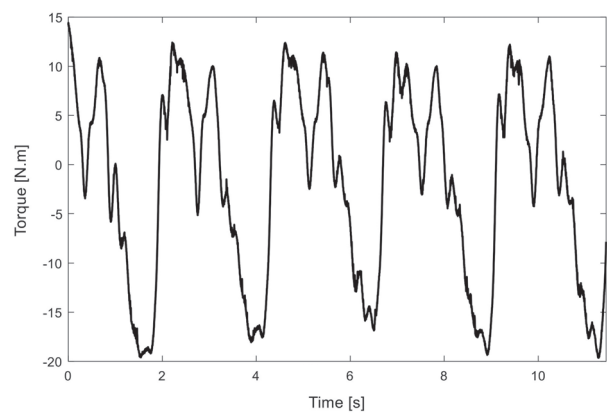Fig. 7.   Tracking a typical hip trajectory in a typical walking with the frequency of 2.63 rad/sec

Fig. 8.   Delivered motor torque during walking with the speed of 2.63 rad/sec

[9] Z. Li, K. Zhao, L. Zhang, X. Wu, T. Zhang, Q. Li, X. Li, and C.-Y. Su, "Human-in-the-loop control of a wearable lower limb exoskeleton for stable dynamic walking," *IEEE/ASME Transactions on Mechatronics*, vol. 26, no. 5, pp. 2700–2711, 2021.

[10] "Rewalk™ personal 6.0 exoskeleton for spinal cord injury," Jun 2021.

[Online]. Available: https://rewalk.com/rewalk-personal-3/

[11] "Ekso bionics webpage." [Online]. Available: https://eksobionics.com/eksonr/

[12] M. Sharifi, V. Azimi, V. K. Mushahwar, and M. Tavakoli, "Impedance learning-based adaptive control for human–robot interaction," *IEEE Transactions on Control Systems Technology*, vol. 30, no. 4, pp. 1345–1358, 2022.
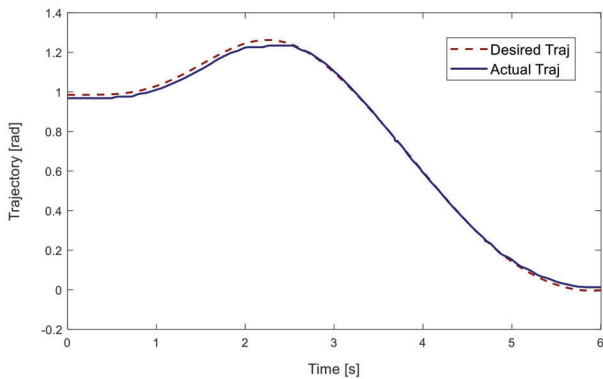
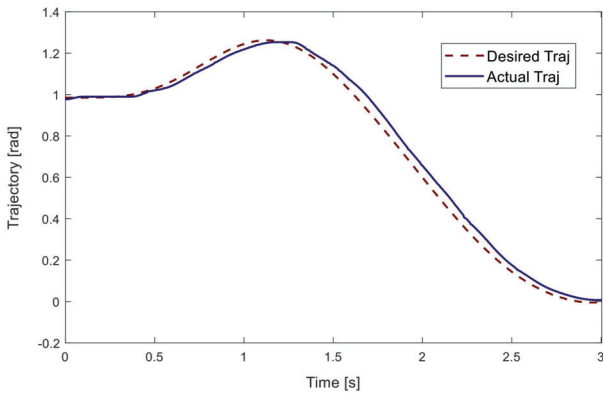Fig. 9. Sit-to-stand trajectory tracking for a 6 sec period

Fig. 10. Sit-to-stand trajectory tracking for a 3 sec period

[13] M. Sharifi, S. Behzadipour, H. Salarieh, and M. Tavakoli, "Assist-as-needed policy for movement therapy using telerobotics-mediated therapist supervision," *Control Engineering Practice*, vol. 101, p. 104481, 2020.

[14] M. Sharifi, A. Zakerimanesh, J. K. Mehr, A. Torabi, V. K. Mushahwar, and M. Tavakoli, "Impedance variation and learning strategies in human–robot interaction," *IEEE Transactions on Cybernetics*, vol. 52, no. 7, pp. 6462–6475, 2022.

[15] Q. Wei, Z. Li, K. Zhao, Y. Kang, and C.-Y. Su, "Synergy-based control of assistive lower-limb exoskeletons by skill transfer," *IEEE/ASME Transactions on Mechatronics*, vol. 25, no. 2, pp. 705–715, 2020.

[16] W. Huo, S. Mohammed, J. C. Moreno, and Y. Amirat, "Lower limb wearable robots for assistance and rehabilitation: A state of the art," *IEEE Systems Journal*, vol. 10, no. 3, pp. 1068–1081, 2016.

[17] M. Oghogho, M. Sharifi, M. Vukadin, C. Chin, V. K. Mushahwar, and M. Tavakoli, "Deep reinforcement learning for emg-based control of assistance level in upper-limb exoskeletons," in *International Symposium on Medical Robotics (ISMR)*, 2022, pp. 1–7.
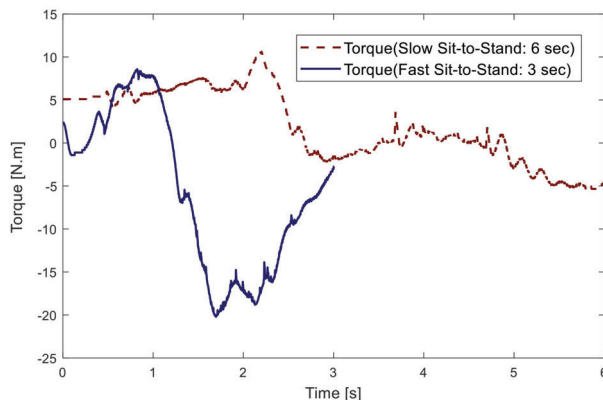
Fig. 11. Applied motor torque for sit-to-stand motion within two time periods (6 sec and 3 sec)

[18] K. Gui, H. Liu, and D. Zhang, "A practical and adaptive method to achieve emg-based torque estimation for a robotic exoskeleton," *IEEE/ASME Transactions on Mechatronics*, vol. 24, no. 2, pp. 483–494, 2019.

[19] ——, "A generalized framework to achieve coordinated admittance control for multi-joint lower limb robotic exoskeleton," in *2017 International Conference on Rehabilitation Robotics (ICORR)*, 2017, pp. 228–233.

[20] S. Qiu, W. Guo, D. Caldwell, and F. Chen, "Exoskeleton online learning and estimation of human walking intention based on dynamical movement primitives," *IEEE Transactions on Cognitive and Developmental Systems*, vol. 13, no. 1, pp. 67–79, 2021.

[21] X. Liu and Q. Wang, "Real-time locomotion mode recognition and assistive torque control for unilateral knee exoskeleton on different terrains," *IEEE/ASME Transactions on Mechatronics*, vol. 25, no. 6, pp. 2722–2732, 2020.

[22] C.-F. Chen, Z.-J. Du, L. He, Y.-J. Shi, J.-Q. Wang, G.-Q. Xu, Y. Zhang, D.-M. Wu, and W. Dong, "Development and hybrid control of an electrically actuated lower limb exoskeleton for motion assistance," *IEEE Access*, vol. 7, pp. 169 107–169 122, 2019.

[23] T. Zhang, M. Tran, and H. Huang, "Design and experimental verification of hip exoskeleton with balance capacities for walking assistance," *IEEE/ASME Transactions on Mechatronics*, vol. 23, no. 1, pp. 274–285, 2018.

[24] D. Zhang, Y. Ren, K. Gui, J. Jia, and W. Xu, "Cooperative control for a hybrid rehabilitation system combining functional electrical stimulation and robotic exoskeleton," *Frontiers in Neuroscience*, vol. 11, 2017. [Online]. Available: https://www.frontiersin.org/articles/10.3389/fnins.2017.00725

[25] R. Huang, H. Cheng, J. Qiu, and J. Zhang, "Learning physical human–robot interaction with coupled cooperative primitives for a lower exoskeleton," *IEEE Transactions on Automation Science and Engineering*, vol. 16, no. 4, pp. 1566–1574, 2019.

[26] R. Luo, S. Sun, X. Zhao, Y. Zhang, and Y. Tang, "Adaptive cpg-based impedance control for assistive lower limb exoskeleton," in *2018 IEEE International Conference on Robotics and Biomimetics (ROBIO)*, 2018, pp. 685–690.

[27] C.-T. Pan, C.-C. Chang, Y.-S. Yang, C.-K. Yen, C.-C. Liu, C.-L. Lee, and Y.-L. Shiue, "Development a multi-loop modulation method on the servo drives for lower limb rehabilitation exoskeleton," *Mechatronics*, vol. 68, p. 102360, 2020. [Online]. Available: https://www.sciencedirect.com/science/article/pii/S0957415820300404

[28] W. Huo, S. Mohammed, and Y. Amirat, "Impedance reduction control of a knee joint human-exoskeleton system," *IEEE Transactions on Control Systems Technology*, vol. 27, no. 6, pp. 2541–2556, 2019.

[29] W. Huo, M. A. Alouane, Y. Amirat, and S. Mohammed, "Force control of sea-based exoskeletons for multimode human–robot interactions," *IEEE Transactions on Robotics*, vol. 36, no. 2, pp. 570–577, 2020.

[30] M. Sharifi, J. K. Mehr, V. K. Mushahwar, and M. Tavakoli, "Autonomous locomotion trajectory shaping and nonlinear control for lower limb exoskeletons," *IEEE/ASME Transactions on Mechatronics*, vol. 27, no. 2, pp. 645–655, 2022.

[31] ——, "Adaptive cpg-based gait planning with learning-based torque estimation and control for exoskeletons," *IEEE Robotics and Automation Letters*, vol. 6, no. 4, pp. 8261–8268, 2021.

[32] "Ak80-64motor." [Online]. Available: https://store.cubemars.com/goods.php?id=1143

[33] Y. M. Pirjade, D. R. Londhe, N. M. Patwardhan, A. U. Kotkar, T. P. Shelke, and S. Ohol, "Design and fabrication of a low-cost human body lower limb exoskeleton," in *2020 6th International Conference on Mechatronics and Robotics Engineering (ICMRE)*, 2020, pp. 32–37.

[34] "Ak series actuator manual." [Online]. Available: https://store.tmotor.com/images/file/202208/251661393360838805.pdf

[35] T. Lencioni, I. Carpinella, M. Rabuffetti, A. Marzegan, and M. Ferrarin, "Human kinematic, kinetic and emg data during different walking and stair ascending and descending tasks," *Scientific data*, vol. 6, no. 1, p. 309, 2019.

[36] S. Nuzik, R. Lamb, A. VanSant, and S. Hirt, "Sit-to-stand movement pattern: a kinematic study," *Physical therapy*, vol. 66, no. 11, pp. 1708–1713, 1986.